

Article

Divergent Metabolomic Signatures of TGF β 2 and TNF α in the Induction of Retinal Epithelial-Mesenchymal Transition

Pei Qin Ng^{1,2,3,4,5} , Magali Saint-Geniez^{2,3}, Leo A. Kim^{2,3} and Daisy Y. Shu^{2,3,*} ¹ Department of Plant Science, University of Cambridge, Downing Street, Cambridge CB2 3EA, Cambridgeshire, UK² Schepens Eye Research Institute of Mass Eye and Ear, Boston, MA 02114, USA³ Department of Ophthalmology, Harvard Medical School, Boston, MA 02114, USA⁴ School of Biological Sciences, The University of Adelaide, Adelaide, SA 5005, Australia⁵ South Australian Health and Medical Research Institute (SAHMRI), Adelaide, SA 5000, Australia

* Correspondence: daisy_shu@meei.harvard.edu

Abstract: Epithelial-mesenchymal transition (EMT) is a dedifferentiation program in which polarized, differentiated epithelial cells lose their cell-cell adhesions and transform into matrix-producing mesenchymal cells. EMT of retinal pigment epithelial (RPE) cells plays a crucial role in many retinal diseases, including age-related macular degeneration, proliferative vitreoretinopathy, and diabetic retinopathy. This dynamic process requires complex metabolic reprogramming to accommodate the demands of this dramatic cellular transformation. Both transforming growth factor-beta 2 (TGF β 2) and tumor necrosis factor-alpha (TNF α) have the capacity to induce EMT in RPE cells; however, little is known about their impact on the RPE metabolome. Untargeted metabolomics using high-resolution mass spectrometry was performed to reveal the metabolomic signatures of cellular and secreted metabolites of primary human fetal RPE cells treated with either TGF β 2 or TNF α for 5 days. A total of 638 metabolites were detected in both samples; 188 were annotated as primary metabolites. Metabolomics profiling showed distinct metabolomic signatures associated with TGF β 2 and TNF α treatment. Enrichment pathway network analysis revealed alterations in the pentose phosphate pathway, galactose metabolism, nucleotide and pyrimidine metabolism, purine metabolism, and arginine and proline metabolism in TNF α -treated cells compared to untreated control cells, whereas TGF β 2 treatment induced perturbations in fatty acid biosynthesis metabolism, the linoleic acid pathway, and the Notch signaling pathway. These results provide a broad metabolic understanding of the bioenergetic rewiring processes governing TGF β 2- and TNF α -dependent induction of EMT. Elucidating the contributions of TGF β 2 and TNF α and their mechanistic differences in promoting EMT of RPE will enable the identification of novel biomarkers for diagnosis, management, and tailored drug development for retinal fibrotic diseases.

Keywords: retinal pigment epithelium (RPE); metabolomics; metabolism; mitochondria; tumor necrosis factor-alpha (TNF α); transforming growth factor-beta (TGF β); epithelial-mesenchymal transition (EMT); OXPHOS; glycolysis; age-related macular degeneration; proliferative vitreoretinopathy



Citation: Ng, P.Q.; Saint-Geniez, M.; Kim, L.A.; Shu, D.Y. Divergent Metabolomic Signatures of TGF β 2 and TNF α in the Induction of Retinal Epithelial-Mesenchymal Transition. *Metabolites* **2023**, *13*, 213. <https://doi.org/10.3390/metabo13020213>

Academic Editor: Chenwei Pan

Received: 31 December 2022

Revised: 23 January 2023

Accepted: 23 January 2023

Published: 31 January 2023



Copyright: © 2023 by the authors. Licensee MDPI, Basel, Switzerland. This article is an open access article distributed under the terms and conditions of the Creative Commons Attribution (CC BY) license (<https://creativecommons.org/licenses/by/4.0/>).

1. Introduction

Epithelial-mesenchymal transition (EMT) is a process in which polarized, differentiated epithelial cells dedifferentiate into matrix-producing mesenchymal cells [1]. This complex biological process is defined by a cascade of cellular and molecular events, including loss of cell–cell adhesions, excessive deposition of extracellular matrix (ECM) proteins, profound cytoskeletal reorganization, increased invasiveness and contractility, and reduced expression of epithelial markers such as E-cadherin and zonula occludens (ZO)-1 [2]. EMT of retinal pigment epithelial (RPE) cells plays an integral role in many retinal pathologies, including dry age-related macular degeneration (AMD) [3–8], wet AMD [9,10], proliferative vitreoretinopathy (PVR) [8,11–14], and diabetic retinopathy (DR) [15].

Metabolic reprogramming has emerged as a prominent hallmark of EMT, particularly in the field of cancer metastasis [16]. Since the seminal observations of the Warburg effect, which found that cancer cells preferentially use glycolysis over mitochondrial oxidative phosphorylation (OXPHOS) for energy generation despite the presence of oxygen [17], numerous examples of dysregulated metabolic pathways in EMT have been documented in glycine metabolism [18], glutamine metabolism [19], the pentose phosphate pathway [19], and lipid metabolism [20]. With significant advances in the field of metabolic reprogramming in EMT during cancer, efforts have been directed towards deciphering the metabolic alterations in retinal EMT. Work in our laboratory has explored the metabolic changes induced by two key EMT inducers: transforming growth factor-beta 2 (TGF β 2) and tumor necrosis factor-alpha (TNF α). While both cytokines potently induce EMT in RPE, they exhibit dramatically distinct bioenergetic profiles: TGF β 2 suppresses mitochondrial respiration and enhances glycolytic capacity [14], whereas TNF α enhances mitochondrial respiration and reduces glycolysis [8].

Both TGF β 2 and TNF α have been implicated in the pathogenesis of AMD. Persistent expression of the TGF β pathway in RPE is associated with choroidal neovascularization and geographic atrophy [3], and a polymorphism in the TGF β receptor type I (TGFBR1) gene is linked to an increased risk of developing AMD [21]. In contrast, TNF α drives the inflammatory component of AMD and mediates the formation of choroidal neovascular membranes by regulating the expression of vascular endothelial growth factor (VEGF) in RPE [22]. Patients with enhanced serum levels of pro-inflammatory cytokines such as interleukin-6 (IL-6) and TNF α respond more favorably to anti-VEGF therapy [23]. Single nucleotide polymorphisms in the TNF α gene have been observed in AMD patients [24].

Among the suite of omics technologies available to elucidate the molecular and biochemical perturbations underpinning retinal EMT, metabolomics is particularly powerful [25]. Metabolomics, defined as the comprehensive analysis of the multitude of native small molecules (metabolites) in a biological specimen, is a rapidly expanding area. Alterations in metabolic fluxes are directly linked to changes in the level of intermediates in affected metabolic pathways and are downstream of changes in gene expression as well as post-transcriptional and post-translational events [16].

In this study, we harnessed the broad scope of untargeted metabolomics to characterize the metabolic reprogramming associated with TNF α - and TGF β 2-induced EMT of RPE. The complete metabolome comprises the endo-metabolome (metabolites within the cell) and the exo-metabolome (metabolites in the extracellular medium) [26]. The untargeted approach enables the generation of an unbiased and comprehensive understanding of how the endo- and exo-metabolome are affected in RPE mesenchymal transition with two distinct stimulators of EMT. In this study, we evaluated both the cellular and media metabolites of H-RPE treated with TNF α or TGF β 2 compared to untreated control H-RPE. We profiled 638 metabolites in both the cellular and secreted metabolome associated with TNF α and TGF β 2 treatments of primary human fetal RPE cells. We aimed to determine the significantly altered metabolites during retinal EMT by comparing the altered metabolite profiles between TNF α -treated or TGF β 2-treated cells vs. untreated control cells as well as differences between the metabolite profiles of TNF α and TGF β 2 treatments.

2. Materials and Methods

2.1. Cell Culture

Primary human fetal RPE (H-RPE, Lonza, Walkersville, MD, USA) were cultured in an RtEGM Retinal Pigment Epithelial Cell Growth Medium supplemented with RtEGM SingleQuots (Lonza, Walkersville, MD, USA), as described previously [8,14]. H-RPE were plated in T25 flasks and maintained in a humidified incubator at 37 °C and 5% CO₂. Cells were passaged 1:3 up to a maximum of 5 passages. Half of the media was changed every two–four days for a month to allow sufficient time for RPE maturation, including pigment accumulation. Cells were tested monthly for mycoplasma contamination (Mycoplasma PCR Test, Applied Biological Materials). Following maturation, cells were serum-starved

for two days before treatment for five days with recombinant human TGF β 2 (Peprotech, Rocky Hill, NJ, USA) or TNF α (Peprotech, Rocky Hill, NJ, USA), both at 10 ng/mL in serum-free media. Growth factors were added freshly each day. This dosage and duration are required for proper mesenchymal transition of H-RPE, as shown in our previous studies [8,14]. Analysis was performed on three groups (control, TGF β 2 and TNF α) with N = 8 in each group.

2.2. Sample Preparation

Sample preparation for analysis of secreted metabolites involved collecting cell culture media (1.5 mL) from each flask and clarifying by centrifugation at 200 \times g for 30 s. One mL of supernatant was transferred into a fresh tube, snap-frozen in liquid nitrogen, and stored at -80 °C until analysis.

For sample preparation of cellular metabolites, H-RPE were rinsed in HEPES-buffered saline and then trypsinized using the ReagentPackTM Subculture Reagents (Lonza, Walkersville, MD, USA) for 5 min in a 37 °C incubator. Cells were then rinsed in trypsin neutralizing solution and centrifuged at 200 \times g for 3.5 min. The cell pellet was rinsed in phosphate buffered saline (PBS), and cells were counted using a hemocytometer. Five million cells per sample were centrifuged at 200 \times g for 3.5 min, and the final cell pellet was snap-frozen in liquid nitrogen and stored at -80 °C until analysis.

2.3. Metabolomics Data Acquisition Using Gas Chromatography Time-of-Flight Mass Spectrometry (GC-TOF MS)

Cellular and media samples were shipped on dry ice to the NIH West Coast Metabolomics Center (UC Davis, LA, USA) for sample processing and analysis as described in [27]. Samples were extracted using 1 mL of 3:3:2 acetonitrile:isopropanol:H₂O (*v/v/v*). Half of the sample was completely dried and then derivatized to increase the volatility and stability for subsequent GC-TOF MS data acquisition. The derivatization process involved adding 10 μ L of 40 mg/mL methoxyamine to pyridine and shaking at 30 °C for 1.5 h. Following this, 91 μ L of a mixture of MSTFA and FAMEs was added to each sample with shaking at 37 °C for 0.5 h to complete derivatization. Samples were then vialled, capped, and injected onto the instrument. Samples were run on a 7890A GC coupled with a LECO TOF. The derivatized sample (0.5 μ L) was injected using a splitless method onto a RESTEK RTX-5SIL MS column with an Integra-Guard at 275 °C with a helium flow of 1 mL/min. The GC oven was set to hold at 50 °C for 1 min and then ramp to 20 °C/min to 330 °C and then hold for 5 min. The transfer line was set to 280 °C, while the EI ion source was set to 250 °C. Metabolites were identified as peaks characterized by mass-over-charge ratio (*m/z*) and retention time. The parameters for mass spectrometry were set to collect data from 85 *m/z* to 500 *m/z* at an acquisition rate of 17 spectra/second. Raw data was deconvoluted using ChromaTOF software v2.32 (LECO Corporation) and processed by the BinBase algorithm for compound identification and quantification.

2.4. Metabolomics Data Analysis

Metabolomics data were first processed using an in-house R script. Processed data were first inspected for sample clustering and variance difference via Principal Component Analysis (PCA) and Partial Least Square Discriminant Analysis (PLSDA), in which PLSDA plots were generated using the R package mixOmics v6.18.1 [28]. Raw *p*-values were adjusted using the Benjamini–Hochberg correction and then tested for significance using the Welch method for metabolite profiling using the R package Omu v1.0.6 [29]. Differential metabolite analysis between the TNF α - and TGF β 2-treated samples compared to control (untreated) samples for both cell and media metabolites was generated by the R package Omu using the *count_fold_change* function, with the log FoldChange (FC) >1.5 or <−1.5 (TNF α -treated H-RPE vs. control H-RPE), logFC > 1.0, and logFC < −1.0 (TGF β 2-treated H-RPE vs. control H-RPE), with a Benjamini–Hochberg adjusted *p*-value cut off < 0.05 [29].

The Enriched Pathway Network Analysis was generated using the KEGG database of *Homo sapiens* [30], which was loaded locally using the functions *buildGraphFromKEGGREST()* and *buildDataFromGraph()* in the R package FELLA v1.14.0 [31]. The lists of metabolites that were significantly different from the TNF α -treated vs. control and TGF β 2-treated vs. control were extracted. The KEGG compound hierarchy was assigned to the extracted list of metabolites for the two comparisons using the function *defineCompounds()* in FELLA by mapping the metabolite compounds against the loaded database. The KEGG-assigned metabolomics data were then used as input for pathway enrichment analysis using the undirected heat diffusion model followed by statistical normalization using Z-scores for sub-network analysis in the R package FELLA v1.14.0 [31]. For the pathway enrichment analysis, metabolites with logFC > 1.5 or < -1.5 (TNF α -treated vs. control), logFC > 1.0, and logFC < -1.0 (TGF β 2-treated vs. control), with a Benjamini–Hochberg adjusted *p*-value < 0.05 were included. The purpose of two different fold-change cutoffs was due to differences in metabolite changes between TNF α -treated and TGF β 2-treated H-RPE, enabling the capture of sufficient differential metabolites in each group for generating a comprehensive network analysis. The enrichment analysis outputs were then mapped to the *Homo sapiens* (hsa) KEGG graphs and subsequently used for network analysis. Optimal visualization of the metabolic network graphs was generated with the number of nodes limit (nlimit) of 250 for TNF α -treated H-RPE vs. control and nlimit of 160 for TGF β 2-treated H-RPE vs. control using the *generateResultsGraph()* in FELLA. KEGG IDs unmapped to the KEGG graphs were retrieved and searched against the KEGG pathway database (<https://www.genome.jp/kegg/pathway.html>, accessed on 28 December 2022).

3. Results

3.1. TNF α - or TGF β 2-Treated H-RPE Exhibited Distinct Cellular Metabolomic Signatures

Principal Component Analysis (PCA) was performed for both cell and media samples to generate clustering patterns of metabolite profiles and detect outliers. For cellular metabolites, three clusters were identified in the PCA score plot (Figure 1A), indicating significant differences between control, TNF α , and TGF β 2. One sample in the TGF β 2 cellular metabolite group was identified as an outlier by cluster analysis and excluded in subsequent analyses. However, for the secreted metabolites, no definitive clusters were observed (Figure S1). We further confirmed the lack of separation between these two groups by performing PLSDA analysis, where overlap occurred between the clusters from media derived from untreated cells (control) and media derived from TNF α and TGF β 2. However, distinct clusters were observed between media samples derived from TNF α - and TGF β 2-treated cells (Figure S1). Analysis of the differential metabolites of media samples showed that for each treatment, only one primary metabolite was significantly different. For media derived from TNF α -treated cells, tartaric acid showed a significant increase compared to media derived from untreated H-RPE cells (logFC > 1.0, *p*-value < 0.05); in media samples derived from TGF β 2-treated cells, isobutylamine showed significant downregulation compared to control (logFC < -1.0, *p*-value < 0.05).

A total of 638 metabolites were detected in both cell metabolite samples; 188 were annotated as primary metabolites and displayed as a heatmap (Figure 1B). A comparison of cellular metabolite changes between TNF α -treated H-RPE and control cells revealed that peptides and organic acids were among the most prominent metabolite classes with significant changes (*p*_{adj} < 0.05, *p*-value < 0.05) at ~30% and ~32% percent, respectively (Figure 1C). Other metabolite classes that showed significant variation following TNF α treatment were vitamins and cofactors (~26%), lipids (~9%), and nucleic acids (~5%). Comparison of cellular metabolite changes between TGF β 2 and control revealed that lipids and organic acids were most prominently affected at ~50% and ~42%, respectively (Figure 1C). Nucleic acids contributed only 9% of the metabolites altered in the TGF β 2 group.

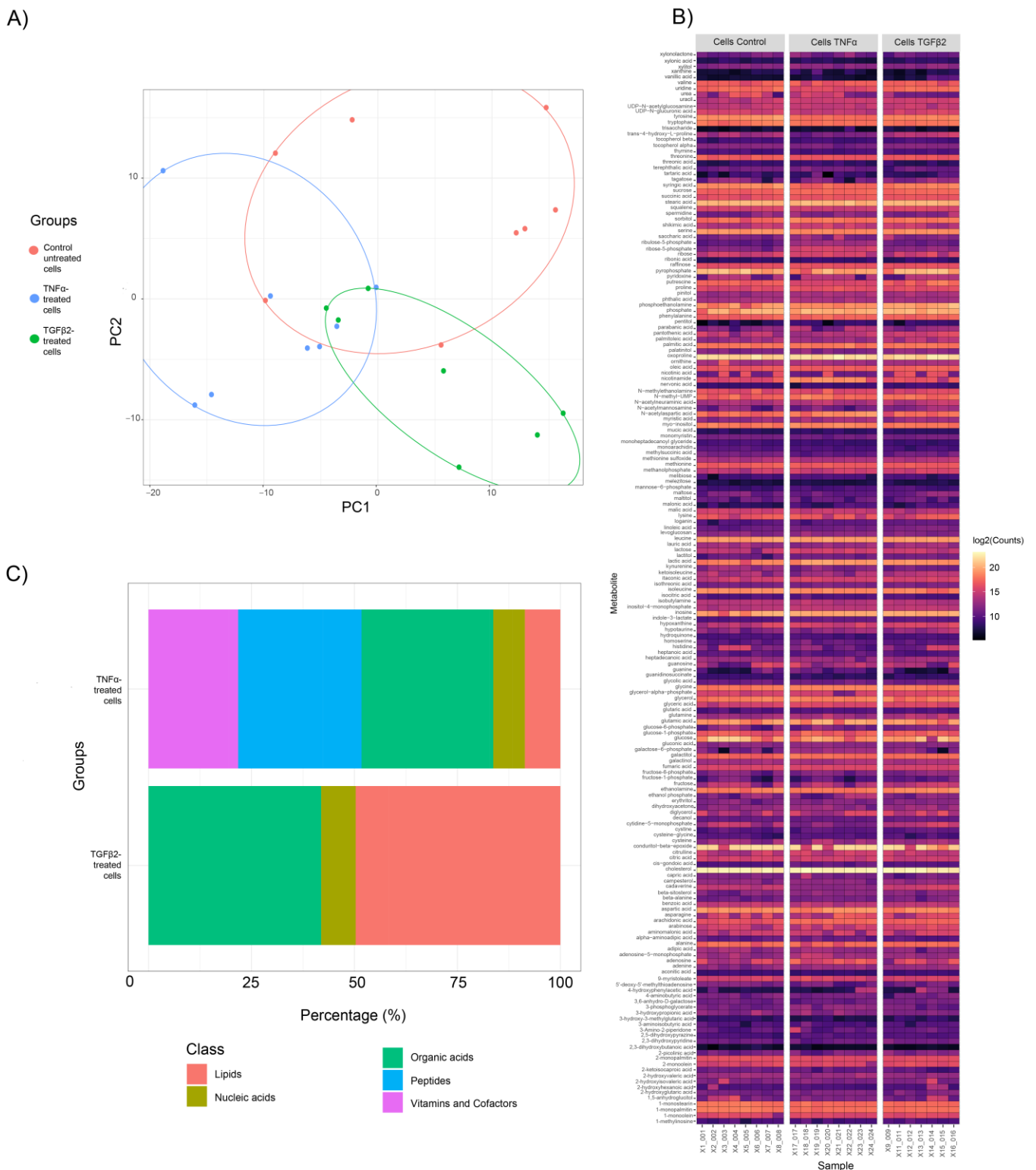


Figure 1. Metabolite profile clustering of TNF α - and TGF β 2-treated H-RPE cells compared to untreated control cells. (A) Principal Component Analysis (PCA) score plots show distinct clusters for samples in the control, TNF α and TGF β 2 cellular metabolite groups. (B) A heatmap of the differential fold changes for all annotated metabolites in each sample analyzed for the three groups. (C) Categorization of differentially expressed metabolites between TNF α - and TGF β 2-treated H-RPE cells compared to untreated control cells.

Since organic acids, nucleic acids, and lipids were common metabolite classes affected in both TNF α and TGF β 2 groups, we examined the compounds in these classes that were significantly changed due to either TNF α - and TGF β 2-treatment (Figure S2). Arachidonic acid (lipid metabolite class) and adenosine (nucleic acid metabolite class) were upregulated in TNF α -treated H-RPE cells, while uridine (nucleic acid metabolite class) was downregulated in TNF α -treated H-RPE cells compared to control. All organic acid compounds (lactic acid, parabanic acid, and malonic acid) were higher in TNF α -treated H-RPE cells compared to control. In TGF β 2-treated H-RPE cells, lipids (linoleic acid and palmitoleic acid) were upregulated, whereas malic acid (organic acid metabolite class) and urea (nucleic acid metabolite class) were downregulated with TGF β 2 treatment compared to control cells.

For visualization of the statistical significance of differential metabolite alterations, volcano plots were generated by comparing the fold change size (x -axis) to the adjusted p value (y -axis) for both TNF α - and TGF β 2-treated cells compared to the control. The plot for TNF α -treated cells highlighted a significant upregulation of galactose 6-phosphate and nicotinamide along with a downregulation of putrescine, uridine, cadaverine, syringic acid, and trans-4-hydroxy-L-proline (Figure 2A). Alterations in these metabolites across each sample in the TNF α and control groups are depicted in the heatmap (Figure 2B).

The volcano plot comparing TGF β 2 to control cells revealed a significant upregulation of linoleic acid and palmitoleic acid as well as a downregulation in malic acid, kynurenine, and urea (Figure 3A), as further depicted in the heatmap (Figure 3B). A comparison of metabolites between TNF α - and TGF β 2-treated cells highlights upregulation of ribose-5-phosphate, ribulose-5-phosphate, nicotinamide, and galactose-6-phosphate in TNF α -treated cells (Figure 4), whereas palmitoleic acid and linoleic acid were upregulated in TGF β 2-treated cells (Figure 4). Uridine, trans-4-hydroxy-L-proline, syringic acid, putrescine, and cadaverine were downregulated in TNF α -treated cells, whereas urea, malic acid, and kynurenine were significantly downregulated in TGF β 2-treated cells (Figure 4).

3.2. Metabolite Pathway Enrichment Analysis Revealed Distinct Regulatory Networks for TNF α and TGF β 2

Metabolite pathway network associations for both TNF α - and TGF β 2-treated cells vs. control were identified and visualized using pathway enrichment analysis. We first performed pathway enrichment followed by network analysis with metabolites by inputting the list of significantly different metabolites in the respective comparisons. In TNF α -treated H-RPE cells, 19 key pathways were enriched (Figure 5A) with 10 compounds. The pentose phosphate pathway (putrescine) and galactose metabolism pathway (D-galactose-6-phosphate), both part of carbohydrate metabolism, were shown to be enriched with TNF α treatment. Other primary enriched pathways included protein digestion and adsorption (cadaverine), the nuclear factor kappa B (NF- κ B) signaling pathway (nicotinamide), Nod-like receptor signaling pathway, base excision repair (nicotinamide), nucleotide and pyrimidine metabolism (uridine), purine metabolism (parabanic acid), and arginine and proline metabolism (trans-4-hydroxy-L-proline). These primary enriched pathways impacted several secondary pathways, such as HIF-1 signaling, apoptosis, and hematopoietic cell lineage pathways (Figure 5A).

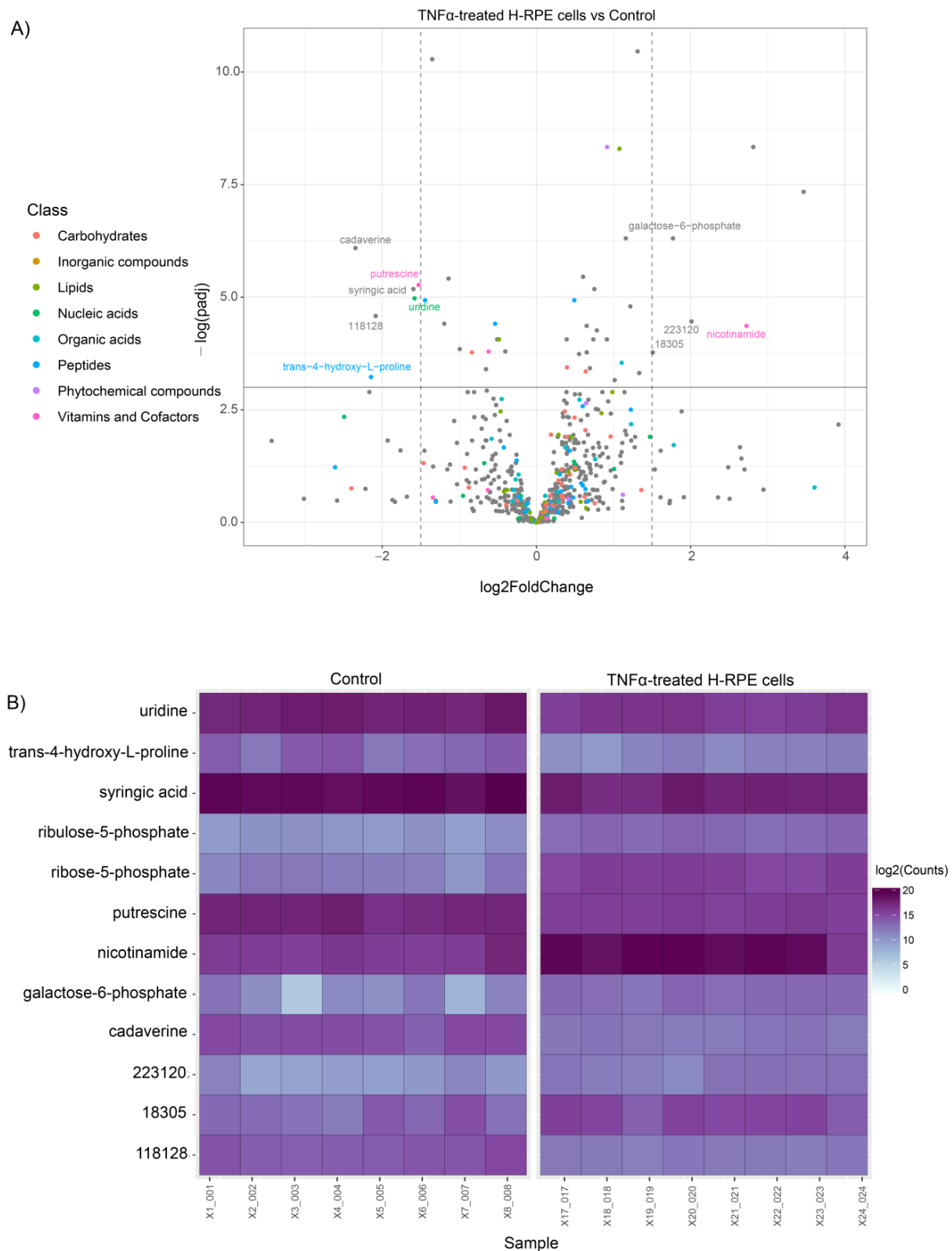


Figure 2. Differential metabolite analysis of TNF α -treated H-RPE cells vs. control. **(A)** A volcano plot illustrating the most significantly altered metabolites relative to fold change and statistical significance. **(B)** A heatmap of the most significantly altered metabolites for each sample analyzed for TNF α vs. control.

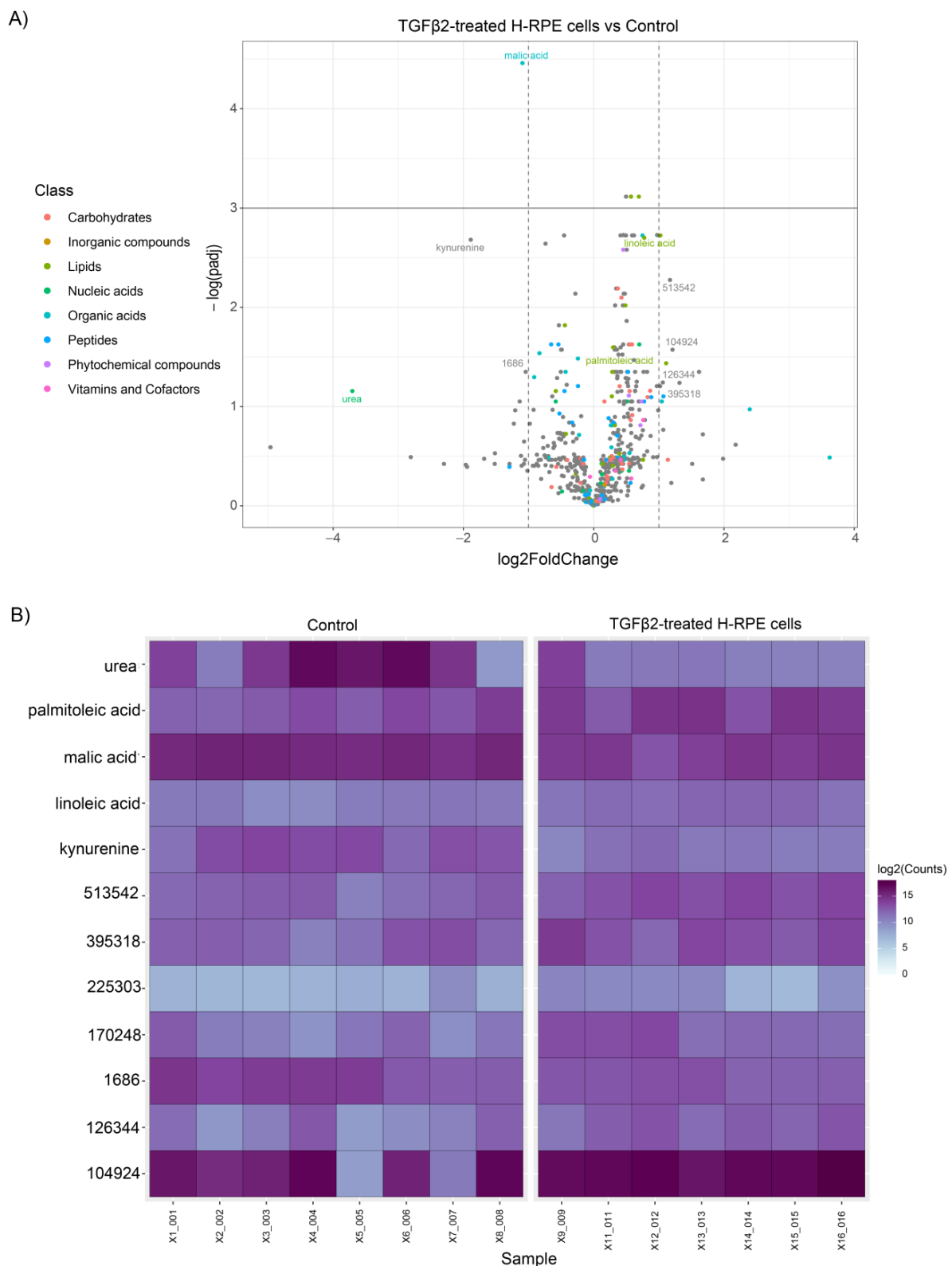


Figure 3. Differential metabolite analysis of TGF β 2-treated H-RPE cells vs. control. **(A)** A volcano plot illustrating the most significantly altered metabolites relative to fold change and statistical significance. **(B)** A heatmap of the most significantly altered metabolites for each sample analyzed for TGF β 2 vs. control.

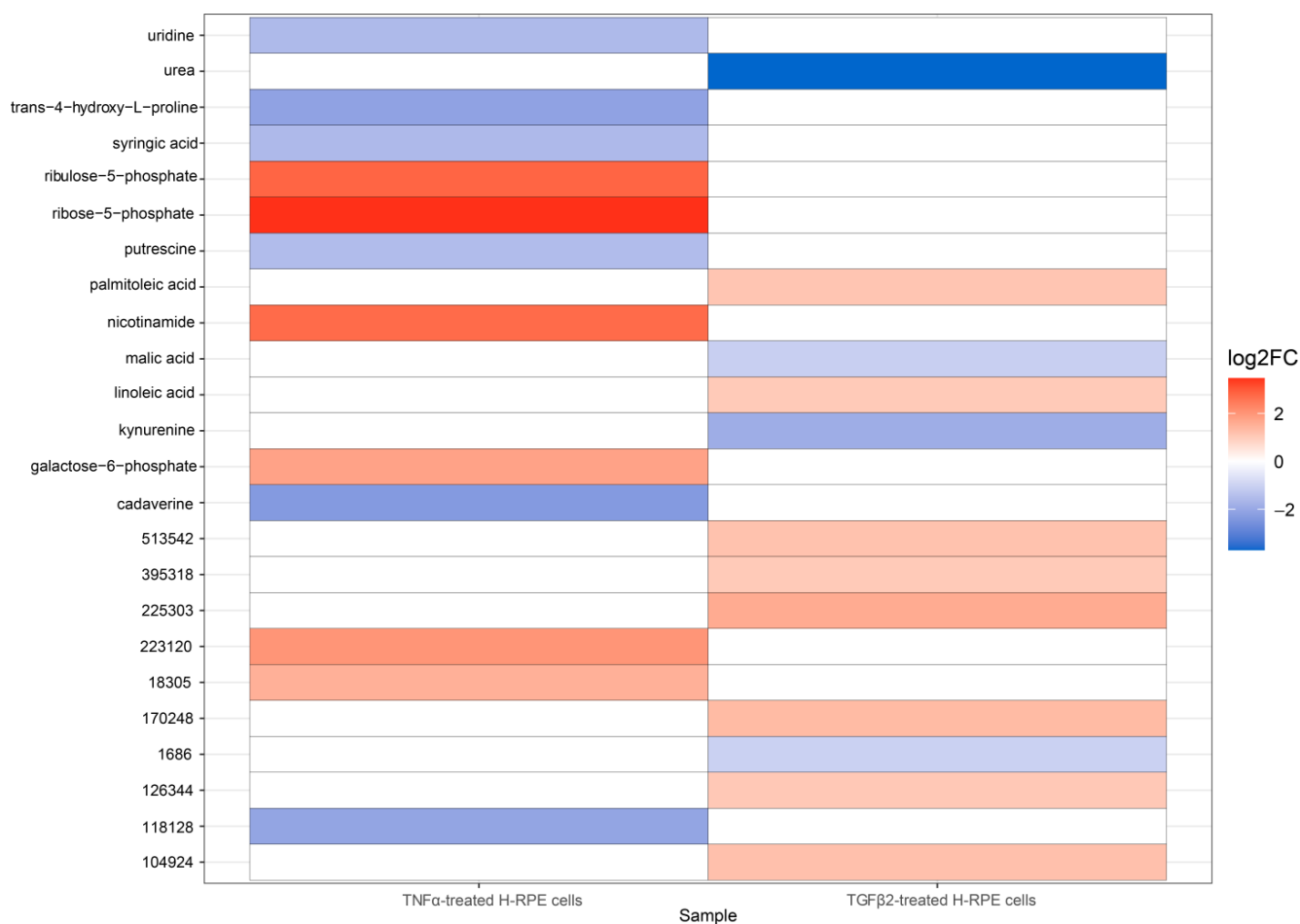


Figure 4. A heatmap depicting differential metabolite changes between TNF α -treated and TGF β 2-treated H-RPE cells. Upregulated metabolites are displayed in red, and downregulated metabolites are displayed in blue. Both annotated (primary) and non-annotated metabolites were included in this analysis. $p_{adj} < 0.05$.

For TGF β 2-treated H-RPE cells, 18 key pathways were enriched in the network analysis with three compounds: urea, linoleic acid, and palmitoleic acid (Figure 5B). Primary pathways directly associated with the altered metabolites were the linoleic acid pathway (linoleic acid), the Notch signaling pathway (urea), and the fatty acid synthesis pathway (palmitoleic acid). These were then shown to impact a cascade of 15 secondary pathways, including the TGF β 2 signaling pathway, Wnt signaling pathway, Hippo signaling pathway, and ubiquitination pathway (Figure 5B).

We further investigated the three compounds that did not directly map onto the hsa KEGG graph within the FELLA package: syringic acid (C10833) for TNF α -treated H-RPE cells as well as kynurenine (C01718) and malate (C00711) for TGF β 2-treated H-RPE cells. These compounds were manually inputted into the KEGG pathway database to render the pathway network. Syringate, a benzoate ester of syringic acid, is part of the aminobenzoate pathway (Figure S3). (S)-malate is involved in glyoxylate and dicarboxylate metabolism, which feeds into the carbohydrate metabolism cycle (Figure S4A). L-kynurenine, an isomer of kynurenine, is involved in the tryptophan signaling pathway (Figure S4B).

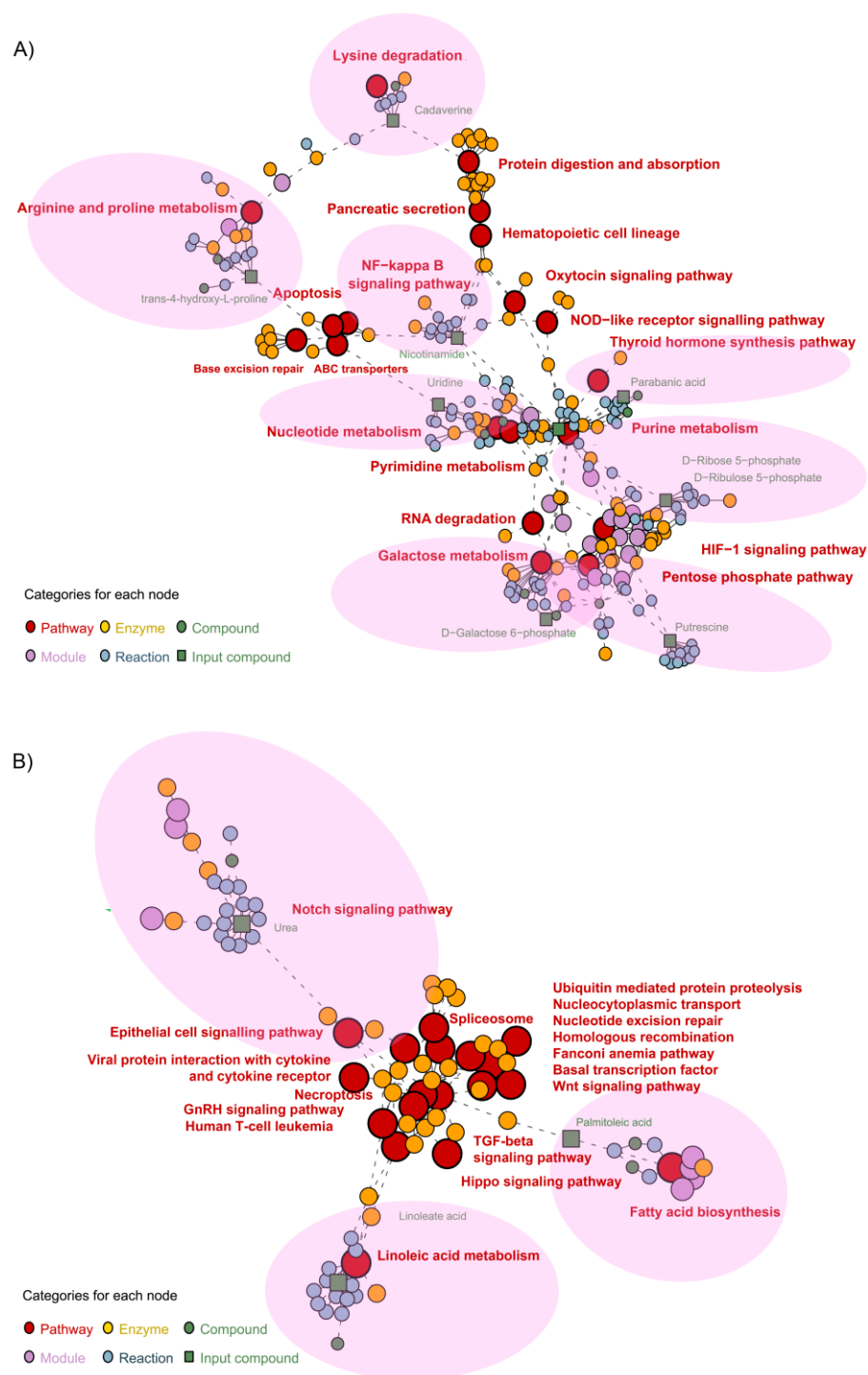


Figure 5. Metabolite pathway enrichment analysis of $\text{TNF}\alpha$ - and $\text{TGF}\beta 2$ -treated H-RPE cells vs. control. Network enrichment analysis of the most differentially expressed metabolites for (A) $\text{TNF}\alpha$ - and (B) $\text{TGF}\beta 2$ -treated H-RPE. Primary pathways affected are indicated by the pink shaded regions.

4. Discussion

EMT is a metabolically demanding process and, as such, requires dramatic reprogramming of cellular metabolism. Here we provide a comprehensive analysis of the metabolomic alterations associated with two potent inducers of EMT in RPE. Despite both inducing EMT, $\text{TNF}\alpha$ and $\text{TGF}\beta 2$ appear to induce divergent metabolic alterations in RPE, highlighting the complexity of the interplay between metabolic reprogramming and EMT. Their divergent metabolomic profiles may be responsible, at least in part, for their differential impact on

inflammation: TNF α induces a robust pro-inflammatory response in RPE [8], whereas TGF β 2 exhibits an anti-inflammatory effect [32].

Inflammation is closely intertwined with metabolic reprogramming. In our study, TNF α upregulated arachidonic acid, an ω -6 polyunsaturated fatty acid, which serves as a precursor to a cascade of pro-inflammatory eicosanoids, including prostaglandins and thromboxanes catalyzed by cyclooxygenase-1 and -2 enzymes, and leukotrienes catalyzed by the 5-lipoxygenase enzyme [33]. Arachidonic acid has been found to reduce the phagocytic capacity of RPE [34], and inhibition of 5-lipoxygenase protects RPE from sodium-iodate-induced degeneration [35]. TNF α can directly stimulate arachidonic acid in neutrophils, perpetuating the inflammatory cascade [36].

Intriguingly, we found that TNF α also significantly increased levels of the anti-inflammatory and antioxidant metabolite, nicotinamide (vitamin B3) [37]. In a metabolomics analysis of plasma samples from AMD patients vs. controls, nicotinamide was found to be significantly altered [38]. Nicotinamide potently suppresses complement activation and inflammation in RPE [39] and enhances mitochondrial metabolism to promote RPE differentiation [40]. A complex relationship exists between nicotinamide and TNF α . Paradoxical increases in levels of nicotinamide adenine dinucleotide (NAD⁺) have been associated with LPS-induced TNF α release in proinflammatory macrophages [41,42] and may be linked to dependence on the NAD⁺ salvage pathway to counteract the increased production of mitochondrial reactive oxygen species (ROS) [43]. It is possible that the increased nicotinamide seen with TNF α in RPE is a compensatory response that prolongs survival in the face of excessive TNF α -induced inflammation and oxidative stress.

Upregulation of the pentose phosphate pathway (PPP) by TNF α in RPE further supports the notion that antioxidants are upregulated to detoxify the increased ROS associated with TNF α . Diverting metabolic substrates from glycolysis into the PPP enables the generation of NADPH for antioxidant defense that serves as a cofactor required by glutathione reductase to reduce oxidized glutathione [44]. Moreover, the PPP supports reductive biosynthesis and ribose biogenesis [45], which are required for the cellular transformation involved in EMT. We also found secondary upregulation of the HIF-1 pathway by TNF α , which is a positive transcriptional regulator of PPP enzymes [46].

Our data showed that TGF β 2 significantly reduces malic acid, a key intermediate metabolite of the TCA cycle, corroborating our previous finding that TGF β 2 suppresses mitochondrial OXPHOS capacity in RPE [14]. In the TCA cycle, the conversion of malate to oxaloacetate is catalyzed by malate dehydrogenase (MDH) using NAD⁺ or NADP⁺ as a cofactor [47]. MDH1 is frequently overexpressed in cancer cells, where it has been shown to enhance glycolysis by replenishing the cytosolic cofactor NAD⁺ [48]. We previously found that exposure to TGF β 2 leads to similar metabolic rewiring with H-RPE showing enhanced glycolysis [14]. In mammals, there is a malate-succinate shuttle between the RPE and neural retina, in which malate exported from the RPE is imported into the retina to fuel succinate production [49,50]. Our data show that suppression of malate by TGF β 2 in RPE in vitro may have significant consequences for neighboring cells in vivo through disruption of the retinal metabolic ecosystem [51].

RPE phagocytose and digest the shed photoreceptor outer segment membranes that are rich in fatty acids [52]. Unsurprisingly, RPE exploit fatty acids as a key energy substrate and are highly dependent on fatty acid metabolism for ATP generation [53]. In this study, TGF β 2 treatment led to decreased levels of both palmitoleic acid and linoleic acid, indicating a disruption in fatty acid metabolism. Dysregulated lipid metabolism has been similarly linked to EMT in cancer; metastatic cells display increased lipolysis, which releases endogenous free fatty acids to generate the reduced form of NADPH through fatty acid oxidation (FAO) [54]. FAO confers a survival advantage for tumor cells by maintaining sufficient energy generation and redox homeostasis, as well as providing a source of lipids for membrane biogenesis [55]. It is possible that TGF β 2-treated RPE overutilize and deplete fatty acid supplies to enable increased FAO.

In conclusion, our results demonstrate the metabolic flexibility of RPE to rapidly adapt and rewire metabolic pathways during the induction of EMT. Despite both inducing EMT, TNF α and TGF β 2 trigger divergent metabolic signatures. While TNF α disrupted metabolic pathways that are involved in inflammation and oxidative stress, including arachidonic acid metabolism and the pentose phosphate pathway, TGF β 2 disrupted the TCA cycle and fatty acid oxidation. With a more complete understanding of the metabolites altered during retinal EMT, we can better comprehend the pathobiology of retinal pathologies such as AMD, PVR, and DR, as well as identify novel biomarkers for diagnosis, prognosis, treatment monitoring, and tailored drug development.

Future investigations will be aimed at exploring the endo- and exo-metabolomic profiles observed in pre-clinical in vivo models of AMD, PVR, and DR. A comparison of the differential metabolite changes from our study on TNF α and TGF β 2 in RPE with data obtained from in vivo models will better inform the individual contributions of these two EMT inducers. Furthermore, studies exploring changes in the metabolome of other retinal cell types involved in AMD, PVR, and DR, including endothelial cells and microglial, following exposure to TNF α and TGF β 2 would be of interest to clarify the contributions of different cell types to metabolomic alterations found in vivo. Identification of key disease-associated metabolic pathways will inform the design of drug screenings to assess the efficacy of novel pharmacotherapies in combating retinal fibrosis.

Supplementary Materials: The following supporting information can be downloaded at: <https://www.mdpi.com/article/10.3390/metabo13020213/s1>, Supplementary Figure S1. Principal Component Analysis (PCA) and Partial Least Squares Discriminant Analysis (PLSDA) score plots for the secreted metabolome following TNF α and TGF β 2 treatment of H-RPE; Supplementary Figure S2. Boxplots for differentially altered metabolites between TNF α -treated and TGF β 2-treated H-RPE compared to untreated control cells. The center line of the boxplot depicts the median values, the upper boundary is the first quartile (Q1), the lower boundary is the third quartile (Q3), and the whiskers represent the highest and lowest values; Supplementary Figure S3. Identification of changes in the aminobenzoate pathway with TNF α -treated H-RPE cells; and Supplementary Figure S4. Identification of changes in the carbohydrate metabolism cycle and tryptophan signaling pathway in TGF β 2-treated H-RPE cells. Supplementary data S1: Raw metabolomics data for control, TNF α -, and TGF β 2-treated samples from cells and media; Supplementary data S2: Differential metabolite analysis results for control, TNF α -, and TGF β 2-treated samples from cells and media; Supplementary data S3: Metadata for pathway enrichment and network analysis of metabolites of control, TNF α -, and TGF β 2-treated samples from cells.

Author Contributions: Conceptualization, M.S.-G. and D.Y.S.; methodology, M.S.-G., P.Q.N. and D.Y.S.; software, P.Q.N. and D.Y.S.; validation, M.S.-G., P.Q.N. and D.Y.S.; formal analysis, M.S.-G., P.Q.N. and D.Y.S.; investigation, M.S.-G., L.A.K., P.Q.N. and D.Y.S.; resources, M.S.-G., L.A.K. and D.Y.S.; data curation, M.S.-G., P.Q.N. and D.Y.S.; writing—original draft preparation, P.Q.N. and D.Y.S.; writing—review and editing, M.S.-G., L.A.K., P.Q.N. and D.Y.S.; visualization, P.Q.N. and D.Y.S.; supervision, M.S.-G., L.A.K. and D.Y.S.; project administration, M.S.-G., L.A.K. and D.Y.S.; funding acquisition, M.S.-G., L.A.K. and D.Y.S. All authors have read and agreed to the published version of the manuscript.

Funding: This study was supported in part by grants from: the Fight for Sight Leonard & Robert Weintraub Postdoctoral Fellowship (D.Y.S.); BrightFocus Foundation Postdoctoral Fellowship Program in Macular Degeneration Research (M2021010F, D.Y.S.); Department of Defense, Spinal Vision Research Program under Award no. VR180132 (M.S.-G. and L.A.K.); National Eye Institute of the National Institutes of Health under Award no. R01EY027739 (L.A.K.); and the Iraty Award (L.A.K.).

Institutional Review Board Statement: Not applicable.

Informed Consent Statement: Not applicable.

Data Availability Statement: All data will be made available upon request. The analysis code can be found on GitHub https://github.com/BioinfoHub-PeiQinNg/RetinalEMT_Metabolomics (accessed on 28 December 2022).

Acknowledgments: We thank Patricia D’Amore for her helpful comments and critical review of this manuscript. Acknowledgment is made to the donors of Macular Degeneration Research, a program of the BrightFocus Foundation, for support of this research. We thank the staff at the West Coast Metabolomics Center for processing our metabolomics samples.

Conflicts of Interest: The authors declare no conflict of interest.

References

1. Shu, D.Y.; Lovicu, F.J. Myofibroblast transdifferentiation: The dark force in ocular wound healing and fibrosis. *Prog. Retin. Eye Res.* **2017**, *60*, 44–65. [[CrossRef](#)]
2. Shu, D.Y.; Butcher, E.; Saint-Geniez, M. EMT and EndMT: Emerging Roles in Age-Related Macular Degeneration. *Int. J. Mol. Sci.* **2020**, *21*, 4271. [[CrossRef](#)]
3. Radeke, M.J.; Radeke, C.M.; Shih, Y.H.; Hu, J.; Bok, D.; Johnson, L.V.; Coffey, P.J. Restoration of mesenchymal retinal pigmented epithelial cells by TGFbeta pathway inhibitors: Implications for age-related macular degeneration. *Genome. Med.* **2015**, *7*, 58. [[CrossRef](#)]
4. Ghosh, S.; Shang, P.; Terasaki, H.; Stepicheva, N.; Hose, S.; Yazdankhah, M.; Weiss, J.; Sakamoto, T.; Bhutto, I.A.; Xia, S.; et al. A Role for β A3/A1-Crystallin in Type 2 EMT of RPE Cells Occurring in Dry Age-Related Macular Degeneration. *Investig. Ophthalmol. Vis. Sci.* **2018**, *59*, Amd104–Amd113. [[CrossRef](#)]
5. Blasiak, J.; Koskela, A.; Pawlowska, E.; Liukkonen, M.; Ruuth, J.; Toropainen, E.; Hyttinen, J.M.T.; Viiri, J.; Eriksson, J.E.; Xu, H.; et al. Epithelial-Mesenchymal Transition and Senescence in the Retinal Pigment Epithelium of NFE2L2/PGC-1alpha Double Knock-Out Mice. *Int. J. Mol. Sci.* **2021**, *22*, 1684. [[CrossRef](#)]
6. Hyttinen, J.M.T.; Kannan, R.; Felszeghy, S.; Niittykoski, M.; Salminen, A.; Kaarniranta, K. The Regulation of NFE2L2 (NRF2) Signalling and Epithelial-to-Mesenchymal Transition in Age-Related Macular Degeneration Pathology. *Int. J. Mol. Sci.* **2019**, *20*, 5800. [[CrossRef](#)]
7. Rosales, M.A.B.; Shu, D.Y.; Iacovelli, J.; Saint-Geniez, M. Loss of PGC-1alpha in RPE induces mesenchymal transition and promotes retinal degeneration. *Life Sci. Alliance* **2019**, *2*, e201800212. [[CrossRef](#)]
8. Shu, D.Y.; Frank, S.I.; Fitch, T.C.; Karg, M.M.; Butcher, E.R.; Nnuji-John, E.; Kim, L.A.; Saint-Geniez, M. Dimethyl Fumarate Blocks Tumor Necrosis Factor-Alpha-Driven Inflammation and Metabolic Rewiring in the Retinal Pigment Epithelium. *Front. Mol. Neurosci.* **2022**, *15*, 896786. [[CrossRef](#)]
9. Lopez, P.F.; Sippy, B.D.; Lambert, H.M.; Thach, A.B.; Hinton, D.R. Transdifferentiated retinal pigment epithelial cells are immunoreactive for vascular endothelial growth factor in surgically excised age-related macular degeneration-related choroidal neovascular membranes. *Investig. Ophthalmol. Vis. Sci.* **1996**, *37*, 855–868.
10. Hirasawa, M.; Noda, K.; Noda, S.; Suzuki, M.; Ozawa, Y.; Shinoda, K.; Inoue, M.; Ogawa, Y.; Tsubota, K.; Ishida, S. Transcriptional factors associated with epithelial-mesenchymal transition in choroidal neovascularization. *Mol. Vis.* **2011**, *17*, 1222–1230.
11. Casaroli-Marano, R.P.; Pagan, R.; Vilaro, S. Epithelial-mesenchymal transition in proliferative vitreoretinopathy: Intermediate filament protein expression in retinal pigment epithelial cells. *Investig. Ophthalmol. Vis. Sci.* **1999**, *40*, 2062–2072.
12. Yang, S.; Li, H.; Li, M.; Wang, F. Mechanisms of epithelial-mesenchymal transition in proliferative vitreoretinopathy. *Discov. Med.* **2015**, *20*, 207–217. [[PubMed](#)]
13. Tamiya, S.; Kaplan, H.J. Role of epithelial-mesenchymal transition in proliferative vitreoretinopathy. *Exp. Eye Res.* **2016**, *142*, 26–31. [[CrossRef](#)] [[PubMed](#)]
14. Shu, D.Y.; Butcher, E.R.; Saint-Geniez, M. Suppression of PGC-1alpha Drives Metabolic Dysfunction in TGFbeta2-Induced EMT of Retinal Pigment Epithelial Cells. *Int. J. Mol. Sci.* **2021**, *22*, 4701. [[CrossRef](#)]
15. Saika, S.; Yamanaka, O.; Okada, Y.; Tanaka, S.; Miyamoto, T.; Sumioka, T.; Kitano, A.; Shirai, K.; Ikeda, K. TGF beta in fibroproliferative diseases in the eye. *Front. Biosci.* **2009**, *1*, 376–390. [[CrossRef](#)]
16. Cherkaoui, S.; Durot, S.; Bradley, J.; Critchlow, S.; Dubuis, S.; Masiero, M.M.; Wegmann, R.; Snijder, B.; Othman, A.; Bendtsen, C.; et al. A functional analysis of 180 cancer cell lines reveals conserved intrinsic metabolic programs. *Mol. Syst. Biol.* **2022**, *18*, e11033. [[CrossRef](#)]
17. Otto, A.M. Warburg effect(s)-a biographical sketch of Otto Warburg and his impacts on tumor metabolism. *Cancer Metab.* **2016**, *4*, 5. [[CrossRef](#)]
18. Jain, M.; Nilsson, R.; Sharma, S.; Madhusudhan, N.; Kitami, T.; Souza, A.L.; Kafri, R.; Kirschner, M.W.; Clish, C.B.; Mootha, V.K. Metabolite profiling identifies a key role for glycine in rapid cancer cell proliferation. *Science* **2012**, *336*, 1040–1044. [[CrossRef](#)]
19. Son, J.; Lyssiotis, C.A.; Ying, H.; Wang, X.; Hua, S.; Ligorio, M.; Perera, R.M.; Ferrone, C.R.; Mullarky, E.; Shyh-Chang, N.; et al. Glutamine supports pancreatic cancer growth through a KRAS-regulated metabolic pathway. *Nature* **2013**, *496*, 101–105. [[CrossRef](#)]
20. Sánchez-Martínez, R.; Cruz-Gil, S.; Gómez de Cedrón, M.; Álvarez-Fernández, M.; Vargas, T.; Molina, S.; García, B.; Herranz, J.; Moreno-Rubio, J.; Reglero, G.; et al. A link between lipid metabolism and epithelial-mesenchymal transition provides a target for colon cancer therapy. *Oncotarget* **2015**, *6*, 38719–38736. [[CrossRef](#)]
21. Fritsche, L.G.; Chen, W.; Schu, M.; Yaspan, B.L.; Yu, Y.; Thorleifsson, G.; Zack, D.J.; Arakawa, S.; Cipriani, V.; Ripke, S.; et al. Seven new loci associated with age-related macular degeneration. *Nat. Genet.* **2013**, *45*, 433–439. [[CrossRef](#)] [[PubMed](#)]

22. Wang, H.; Han, X.; Wittchen, E.S.; Hartnett, M.E. TNF- α mediates choroidal neovascularization by upregulating VEGF expression in RPE through ROS-dependent β -catenin activation. *Mol. Vis.* **2016**, *22*, 116–128. [[PubMed](#)]
23. Nassar, K.; Grisanti, S.; Elfar, E.; Lücke, J.; Lücke, M.; Grisanti, S. Serum cytokines as biomarkers for age-related macular degeneration. *Graefes. Arch. Clin. Exp. Ophthalmol.* **2015**, *253*, 699–704. [[CrossRef](#)]
24. Wan, L.; Lin, H.J.; Tsai, Y.; Lee, C.C.; Tsai, C.H.; Tsai, F.J.; Tsai, Y.Y.; Lin, J.M. Tumor necrosis factor-alpha gene polymorphisms in age-related macular degeneration. *Retina* **2010**, *30*, 1595–1600. [[CrossRef](#)]
25. Wishart, D. Metabolomics and the Multi-Omics View of Cancer. *Metabolites* **2022**, *12*, 154. [[CrossRef](#)]
26. Leon, Z.; Garcia-Canaveras, J.C.; Donato, M.T.; Lahoz, A. Mammalian cell metabolomics: Experimental design and sample preparation. *Electrophoresis* **2013**, *34*, 2762–2775. [[CrossRef](#)] [[PubMed](#)]
27. Fiehn, O. Metabolomics by Gas Chromatography-Mass Spectrometry: Combined Targeted and Untargeted Profiling. *Curr. Protoc. Mol. Biol.* **2016**, *114*, 30.34.31–30.34.32. [[CrossRef](#)]
28. Rohart, F.; Gautier, B.; Singh, A.; KA, L.C. mixOmics: An R package for ‘omics feature selection and multiple data integration. *PLoS Comput. Biol.* **2017**, *13*, e1005752. [[CrossRef](#)]
29. Tiffany, C.R.; Baumler, A.J. omu, a Metabolomics Count Data Analysis Tool for Intuitive Figures and Convenient Metadata Collection. *Microbiol. Resour. Announc.* **2019**, *8*, e00129. [[CrossRef](#)]
30. Kanehisa, M.; Sato, Y.; Kawashima, M.; Furumichi, M.; Tanabe, M. KEGG as a reference resource for gene and protein annotation. *Nucleic Acids Res.* **2016**, *44*, D457–D462. [[CrossRef](#)]
31. Picart-Armada, S.; Fernandez-Albert, F.; Vinaixa, M.; Yanes, O.; Perera-Lluna, A. FELLA: An R package to enrich metabolomics data. *BMC Bioinform.* **2018**, *19*, 538. [[CrossRef](#)] [[PubMed](#)]
32. Paglinawan, R.; Malipiero, U.; Schlapbach, R.; Frei, K.; Reith, W.; Fontana, A. TGFbeta directs gene expression of activated microglia to an anti-inflammatory phenotype strongly focusing on chemokine genes and cell migratory genes. *Glia* **2003**, *44*, 219–231. [[CrossRef](#)] [[PubMed](#)]
33. Hanna, V.S.; Hafez, E.A.A. Synopsis of arachidonic acid metabolism: A review. *J. Adv. Res.* **2018**, *11*, 23–32. [[CrossRef](#)] [[PubMed](#)]
34. Tripathi, B.J.; Tripathi, R.C. Effect of arachidonic acid on normal and dystrophic retinal pigment epithelium in tissue culture. *Investig. Ophthalmol. Vis. Sci.* **1981**, *20*, 553–557.
35. Lee, J.J.; Chang-Chien, G.P.; Lin, S.; Hsiao, Y.T.; Ke, M.C.; Chen, A.; Lin, T.K. 5-Lipoxygenase Inhibition Protects Retinal Pigment Epithelium from Sodium Iodate-Induced Ferroptosis and Prevents Retinal Degeneration. *Oxidative Med. Cell. Longev.* **2022**, *2022*, 1792894. [[CrossRef](#)]
36. Robinson, B.S.; Hii, C.S.; Poulos, A.; Ferrante, A. Effect of tumor necrosis factor-alpha on the metabolism of arachidonic acid in human neutrophils. *J. Lipid Res.* **1996**, *37*, 1234–1245. [[CrossRef](#)]
37. Maiese, K.; Chong, Z.Z.; Hou, J.; Shang, Y.C. The vitamin nicotinamide: Translating nutrition into clinical care. *Molecules* **2009**, *14*, 3446–3485. [[CrossRef](#)]
38. Lains, I.; Chung, W.; Kelly, R.S.; Gil, J.; Marques, M.; Barreto, P.; Murta, J.N.; Kim, I.K.; Vavvas, D.G.; Miller, J.B.; et al. Human Plasma Metabolomics in Age-Related Macular Degeneration: Meta-Analysis of Two Cohorts. *Metabolites* **2019**, *9*, 127. [[CrossRef](#)]
39. Saini, J.S.; Corneo, B.; Miller, J.D.; Kiehl, T.R.; Wang, Q.; Boles, N.C.; Blenkinsop, T.A.; Stern, J.H.; Temple, S. Nicotinamide Ameliorates Disease Phenotypes in a Human iPSC Model of Age-Related Macular Degeneration. *Cell Stem Cell* **2017**, *20*, 635–647.e7. [[CrossRef](#)]
40. Hazim, R.A.; Paniagua, A.E.; Tang, L.; Yang, K.; Kim, K.K.O.; Stiles, L.; Divakaruni, A.S.; Williams, D.S. Vitamin B3, nicotinamide, enhances mitochondrial metabolism to promote differentiation of the retinal pigment epithelium. *J. Biol. Chem.* **2022**, *298*, 102286. [[CrossRef](#)]
41. Al-Shabany, A.J.; Moody, A.J.; Foey, A.D.; Billington, R.A. Intracellular NAD⁺ levels are associated with LPS-induced TNF-alpha release in pro-inflammatory macrophages. *Biosci. Rep.* **2016**, *36*, e00301. [[CrossRef](#)]
42. Iqbal, J.; Zaidi, M. TNF regulates cellular NAD⁺ metabolism in primary macrophages. *Biochem. Biophys. Res. Commun.* **2006**, *342*, 1312–1318. [[CrossRef](#)] [[PubMed](#)]
43. Cameron, A.M.; Castoldi, A.; Sanin, D.E.; Flachsmann, L.J.; Field, C.S.; Puleston, D.J.; Kyle, R.L.; Patterson, A.E.; Hässler, F.; Buescher, J.M.; et al. Inflammatory macrophage dependence on NAD(+) salvage is a consequence of reactive oxygen species-mediated DNA damage. *Nat. Immunol.* **2019**, *20*, 420–432. [[CrossRef](#)]
44. Chen, L.; Zhang, Z.; Hoshino, A.; Zheng, H.D.; Morley, M.; Arany, Z.; Rabinowitz, J.D. NADPH production by the oxidative pentose-phosphate pathway supports folate metabolism. *Nat. Metab.* **2019**, *1*, 404–415. [[CrossRef](#)] [[PubMed](#)]
45. Jiang, P.; Du, W.; Wu, M. Regulation of the pentose phosphate pathway in cancer. *Protein Cell* **2014**, *5*, 592–602. [[CrossRef](#)] [[PubMed](#)]
46. Tokuda, K.; Baron, B.; Yamashiro, C.; Kuramitsu, Y.; Kitagawa, T.; Kobayashi, M.; Sonoda, K.H.; Kimura, K. Up-regulation of the pentose phosphate pathway and HIF-1alpha expression during neural progenitor cell induction following glutamate treatment in rat ex vivo retina. *Cell Biol. Int.* **2019**, *44*, 137–144. [[CrossRef](#)] [[PubMed](#)]
47. Eniafe, J.; Jiang, S. The functional roles of TCA cycle metabolites in cancer. *Oncogene* **2021**, *40*, 3351–3363. [[CrossRef](#)] [[PubMed](#)]
48. Hanse, E.A.; Ruan, C.; Kachman, M.; Wang, D.; Lowman, X.H.; Kelekar, A. Cytosolic malate dehydrogenase activity helps support glycolysis in actively proliferating cells and cancer. *Oncogene* **2017**, *36*, 3915–3924. [[CrossRef](#)] [[PubMed](#)]
49. Bisbach, C.M.; Hass, D.T.; Robbins, B.M.; Rountree, A.M.; Sadilek, M.; Sweet, I.R.; Hurley, J.B. Succinate Can Shuttle Reducing Power from the Hypoxic Retina to the O(2)-Rich Pigment Epithelium. *Cell Rep.* **2020**, *31*, 107606. [[CrossRef](#)] [[PubMed](#)]

50. Hass, D.T.; Bisbach, C.M.; Robbins, B.M.; Sadilek, M.; Sweet, I.R.; Hurley, J.B. Succinate metabolism in the retinal pigment epithelium uncouples respiration from ATP synthesis. *Cell Rep.* **2022**, *39*, 110917. [[CrossRef](#)]
51. Hurley, J.B. Retina Metabolism and Metabolism in the Pigmented Epithelium: A Busy Intersection. *Annu. Rev. Vis. Sci.* **2021**, *7*, 665–692. [[CrossRef](#)] [[PubMed](#)]
52. Lakkaraju, A.; Umapathy, A.; Tan, L.X.; Daniele, L.; Philp, N.J.; Boesze-Battaglia, K.; Williams, D.S. The cell biology of the retinal pigment epithelium. *Prog. Retin. Eye Res.* **2020**, *78*, 100846. [[CrossRef](#)] [[PubMed](#)]
53. Adijanto, J.; Du, J.; Moffat, C.; Seifert, E.L.; Hurle, J.B.; Philp, N.J. The retinal pigment epithelium utilizes fatty acids for ketogenesis. *J. Biol. Chem.* **2014**, *289*, 20570–20582. [[CrossRef](#)] [[PubMed](#)]
54. Koundouros, N.; Poulogiannis, G. Reprogramming of fatty acid metabolism in cancer. *Br. J. Cancer* **2020**, *122*, 4–22. [[CrossRef](#)] [[PubMed](#)]
55. Capece, D.; Franzoso, G. Rewired lipid metabolism as an actionable vulnerability of aggressive colorectal carcinoma. *Mol. Cell. Oncol.* **2022**, *9*, 2024051. [[CrossRef](#)] [[PubMed](#)]

Disclaimer/Publisher’s Note: The statements, opinions and data contained in all publications are solely those of the individual author(s) and contributor(s) and not of MDPI and/or the editor(s). MDPI and/or the editor(s) disclaim responsibility for any injury to people or property resulting from any ideas, methods, instructions or products referred to in the content.